Analytical and Experimental Characterization of Macro-Fiber Composite Actuated Thin Clamped-Free Unimorph Benders

Onur Bilgen[1]
e-mail: onurb@vt.edu

Alper Erturk

Daniel J. Inman

Center for Intelligent Material Systems and Structures,
Virginia Tech,
310 Durham Hall,
Blacksburg, VA 24061;
Department of Mechanical Engineering,
Virginia Tech,
310 Durham Hall,
Blacksburg, VA 24061

A type of piezoceramic composite actuator known as Macro-Fiber Composite (MFC) is used commonly for actuation in smart-material structures. In this paper, a linear distributed parameter electromechanical model is proposed to predict the structural response to MFC actuated clamped-free thin cantilevered beams. The structural frequency response behavior between the tip velocity of the cantilever beam and the actuation voltage of the piezoelectric material is investigated experimentally for cantilevered unimorph MFC actuated benders with aluminum, brass, and steel substrate materials with different thicknesses. Good correlation is observed between the model and the experimental observations. [DOI: 10.1115/1.4001504]

Keywords: piezocomposite actuators, unimorph, clamped-free, actuation model, MFC

1 Introduction

The past few decades have seen the development and integration of active materials into a variety of host structures as a superior means of measuring and controlling its behavior. Piezoceramics remain the most widely used "smart" or active material because they offer high actuation and sensing capability over a wide range of frequencies. Specifically, piezoceramic materials have been extensively studied and employed in aerospace structures by performing shape and flow control. Macro-Fiber Composite (MFC) is a type of piezoceramic material that offers structural flexibility and high actuation authority. A common disadvantage with piezoceramic actuators and with the MFC actuator is that they require high-voltage input. A MFC actuator has a typical voltage input range of −500 V to 1500 V. In contrast, the current drain is usually low, creating reasonable power consumption. With the continuing development in the electronic systems, active materials become feasible in small aerodynamic applications such as small unmanned aerial vehicles (UAVs) and micro aerial vehicles (MAVs).

The Macro-Fiber Composite was developed at NASA Langley Research Center [1,2]. A MFC is a layered, planar actuation device that employs rectangular cross section, unidirectional piezoceramic fibers. The in-plane poling and subsequent voltage actuation allows the MFC to utilize the d_{33} piezoelectric effect, which is much stronger than the d_{31} effect used by traditional lead zirconate titanate (PZT) actuators with through-the-thickness poling [3]. There have been extensive analytical and experimental researches focused on utilizing MFC as an actuator (or sensor) for structural control. Williams [4] provided a detailed nonlinear characterization of the mechanical and piezoelectric behavior of the MFC actuator.

The weight benefit and bandwidth of a smart-material actuator makes it ideal for small aircraft applications. The use of conformal, zero mass flux actuators in aerodynamic flow control has been presented recently as a novel means of controlling laminar separation bubble (LSB) on small aircraft subjected to low Reynolds number flows. Conformal zero mass flux actuators include synthetic jets [5], plasma actuators [6], and piezoceramic actuators that move in the out-of-plane direction [7]. The motivation for designing such an actuator is to increase the bandwidth of the actuation, where the ability to re-attach the LSB is dependent on the excitation frequency.

Kim and Han [8] designed and fabricated a smart flapping wing by using a graphite/epoxy composite material and a MFC actuator. This paper was aimed to mimic the flapping motion of birds. A 20% increase in the lift was achieved in wind tunnel by changing the camber of the wing at different stages of flapping motion.

Moses et al. [9] used both active fiber composite (AFC, which is an earlier version of MFC) and MFC to actively reduce vibration levels in the tail fins of a wind-tunnel model of a fighter jet subjected to buffet loads. The fin-tip peak acceleration was reduced by about 70% with the MFCs and about 85% with the AFCs at frequencies near the first bending mode.

Recently, Bilgen, et al. [10,11] presented a new application for piezocomposite actuators on a 0.76 m wingspan morphing wing air vehicle with approximately 0.815 kg total weight. In this application, two MFC patches are bonded to the wings, and the camber of the wing is changed with the actuator voltage. The aircraft demonstrated that lightweight, conformal actuators can be used as primary control surfaces on an aircraft. All electronics, including MFC power electronics (103 g), are powered by an 11.1 V lithium-polymer battery (106 g). The aircraft uses a 150 W brushless motor for thrust; in contrast, the MFC power electronics consume only 3.0 W during maximum morphing.

This paper extends the authors' previous work by modeling and experimentally evaluating thin unimorph actuators. First, analytical model of a MFC actuated thin clamped-free beam is presented. Next, the model prediction of the tip-velocity frequency response function is compared with the experimental values. This paper concludes with a brief discussion of the results and the authors' future research in the area.

2 Electromechanical Model for Transverse Vibration Response

In order to predict the transverse vibration response of a cantilevered MFC unimorph due to a dynamic voltage excitation, a distributed parameter formulation is employed here [12]. Since the interdigitated electrodes have a negligible thickness and the

[1]Corresponding author.

Contributed by the Technical Committee on Vibration and Sound of ASME for publication in the JOURNAL OF VIBRATION AND ACOUSTICS. Manuscript received May 15, 2009; final manuscript received March 15, 2010; published online August 19, 2010. Assoc. Editor: Michael Brennan.

beam cross section is small with respect to the bending wavelength at the highest frequency of interest, the unimorph cantilever is modeled as a uniform Euler–Bernoulli beam. The MFCs studied here operate in the d_{33} mode of piezoelectricity, and the respective (well-known) constitutive relation is

$$T_3 = c_{33}^E S_3 - e_{33} E_3 \tag{1}$$

where T_3 is the stress component, S_3 is the strain component, E_3 is the electric field component, e_{33} is the piezoelectric constant, and c_{33}^E is elastic stiffness component at constant electric field (reduced for the thin beam theory).

Undamped free vibrations of the beam are governed by

$$\frac{\partial^2 M(x,t)}{\partial x^2} + c_s I \frac{\partial^5 w(x,t)}{\partial x^4 \partial t} + c_a \frac{\partial w(x,t)}{\partial t} + m \frac{\partial^2 w(x,t)}{\partial t^2} = 0 \tag{2}$$

where $M(x,t)$ is the internal bending moment (excluding the strain rate effect), $w(x,t)$ is the transverse deflection, I is the cross section area moment of inertia, $c_s I$ is the Kelvin–Voigt damping term, c_a is the viscous damping coefficient, and m is the mass per unit length of the beam. After expressing the strain component in terms of the curvature and the electric field in terms of the voltage $(E_3(t) = -v(t)/\Delta_{\text{el}}$, where $v(t)$ is the voltage across the interdigitated electrodes and Δ_{el} is the effective electrode spacing) one can integrate the moment of Eq. (1) and substitute in Eq. (2) to obtain the coupled equation for the forced vibrations of the beam

$$YI \frac{\partial^4 w(x,t)}{\partial x^4} + c_s I \frac{\partial^5 w(x,t)}{\partial x^4 \partial t} + c_a \frac{\partial w(x,t)}{\partial t} + m \frac{\partial^2 w(x,t)}{\partial t^2} = -v(t) \frac{d^2 \Gamma(x)}{dx^2} \tag{3}$$

where YI is the bending stiffness (obtained from the transformed cross-section) and $\Gamma(x)$ accounts for the spatial distribution of the electric potential [13]

$$\Gamma(x) = \vartheta \sum_{i=1}^{N_e} \left\{ \left(1 + \frac{x - x_{i0}}{x_{i0} - x_{i1}} \right) [H(x - x_{i0}) - H(x - x_{i1})] + \left(\frac{x - x_{i2}}{x_{i3} - x_{i2}} \right) [H(x - x_{i2}) - H(x - x_{i3})] \right\} \tag{4}$$

where N_e is the number of electrode pairs over the beam length $(N_e \cong L_{\text{act}}/2(u_e + u_0)$, where L_{act} is the active beam length, u_e is the width of each electrode in the direction of the beam axis, u_0 is the width of each nonelectroded region in the direction of the beam axis), $H(x)$ is the Heaviside function, and ϑ is a coupling constant, which will be discussed later. At an arbitrary instant of the motion, the electric potential is assumed to be linearly decreasing from $v(t)$ to 0 in $x_{i0} \le x \le x_{i1}$, whereas it is assumed to be linearly increasing from 0 to $v(t)$ in $x_{i2} \le x \le x_{i3}$. The coupling treatment given by Eq. (2) is a summation of N_e terms due to the piezoelectric coupling on small fiber elements under the electric field applied. Therefore, the positions x_{i0}, x_{i1}, x_{i2}, and x_{i3} change with the index i. As one moves from the clamped end to the free end, the index number increases. For instance, starting from the clamped end, i.e., for $i=1$

$$x_{10} = \frac{u_e}{4}, \quad x_{11} = x_{10} + u_0 + \frac{u_e}{2}, \qquad x_{12} = x_{11} + \frac{u_e}{2}, \quad x_{13} = x_{12} + u_0 + \frac{u_e}{2} \tag{5}$$

and so on for $i = 1 \ldots N_e$ with the increasing index number until the end of the active length. Figure 1 shows the index scheme for the electrodes.

The effective electrode spacing is calculated by $\Delta_{\text{el}} = u_0 + u_e/2$. In Eq. (2), the coupling constant is given by:

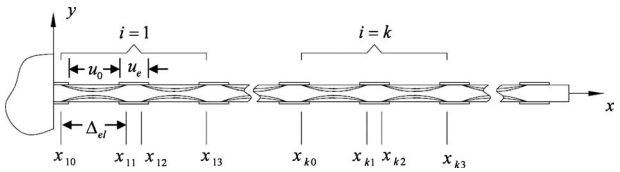

Fig. 1 Geometric parameters of the piezoceramic fibers used in the coupling term (substrate is excluded)

$$\vartheta = -\frac{e_{33} b_{\text{pt}} [(h_d - \alpha h_p)^2 - (h_c + \alpha h_p)^2]}{2\Delta_{\text{el}}} \tag{6}$$

where e_{33} is the piezoelectric constant (reduced for the thin beam theory), b_{pt} is the total width of the piezoceramic fibers, h_p is the thickness of the piezoceramic fibers, h_c is the position of the bottom of the piezoceramic layer from the neutral axis, and h_d is the position of the top of the piezoceramic layer from the neutral axis. Note that the electric field is assumed to be uniform over the effective electrode spacing Δ_{el}. The form of the coupling constant given by Eq. (4) is similar to the coupling constant given for a unimorph cantilever with a monolithic ceramic, where the electric field is uniform and the d_{31} mode is used instead of the d_{33} mode with nonuniform electric field in reality [12]. In Eq. (4), α is an empirical constant that reduces the thickness of the piezoceramic to an effective value due to a nonuniform electric field. An average value of $\alpha = 0.20$ is identified by matching the model predictions for a set of experiments using M8507 P1 type MFC with different substrates.

The solution of Eq. (1) can be expressed as

$$w(x,t) = \sum_{r=1}^{\infty} \phi_r(x) \eta_r(t) \tag{7}$$

where $\phi_r(x)$ and $\eta_r(t)$ are the mass normalized eigenfunction and the modal response of the clamped-free beam for the rth mode, respectively. For a proportionally damped system, the mass normalized eigenfunctions denoted by $\phi_r(x)$ are given by

$$\phi_r(x) = \sqrt{\frac{1}{mL}} \left[\cosh \frac{\lambda_r}{L} x - \cos \frac{\lambda_r}{L} x - \sigma_r \left(\sinh \frac{\lambda_r}{L} x - \sin \frac{\lambda_r}{L} x \right) \right] \tag{8}$$

where the dimensionless frequency numbers (λ_r) are obtained from

$$1 + \cos \lambda_r \cosh \lambda_r = 0 \tag{9}$$

and σ_r is expressed as

$$\sigma_r = \frac{\sinh \lambda_r - \sin \lambda_r}{\cosh \lambda_r + \cos \lambda_r} \tag{10}$$

Moreover, ω_r is the undamped natural frequency of the rth mode

$$\omega_r = \lambda_r^2 \sqrt{\frac{YI}{mL^4}} \tag{11}$$

which is approximately the resonance frequency (for light mechanical damping) of the unimorph when the electrodes are shorted. The eigenfunctions satisfy the following orthogonality conditions:

$$\int_{x=0}^{L} m \phi_s(x) \phi_r(x) dx = \delta_{rs}, \quad \int_{x=0}^{L} YI \phi_s(x) \frac{d^4 \phi_r(x)}{dx^4} dx = \omega_r^2 \delta_{rs} \tag{12}$$

Using Eq. (7) in Eq. (3) and applying the orthogonality conditions of the eigenfunctions gives the electromechanically coupled ordinary differential equation for the modal response of the beam as

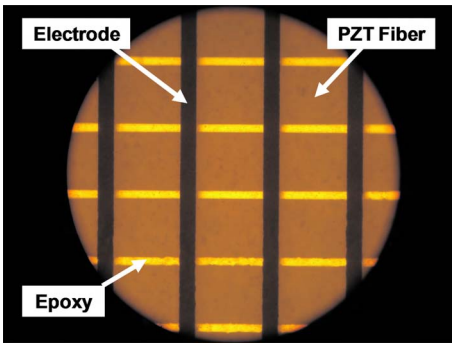

Fig. 2 Digital photograph of the planar view of a MFC 8507-P1 actuator under a microscope

$$\frac{d^2\eta_r(t)}{dt^2} + 2\zeta_r\omega_r\frac{d\eta_r(t)}{dt} + \omega_r{}^2\eta_r(t) = -\chi_r v(t) \tag{13}$$

where

$$\chi_r = \vartheta\sum_{i=1}^{N_e}\left(\frac{\phi_r(x_{i0}) - \phi_r(x_{i1})}{x_{i0} - x_{i1}} + \frac{\phi_r(x_{i2}) - \phi_r(x_{i3})}{x_{i3} - x_{i2}} + \left.\frac{d\phi_r(x)}{dx}\right|_{x_{i0}}^{x_{i3}}\right) \tag{14}$$

and based on the proportional damping assumption, ζ_r is the modal mechanical damping ratio and it is related to the physical damping parameter through

$$\zeta_r = \frac{c_s I\omega_r}{2YI} + \frac{c_a}{2m\omega_r} \tag{15}$$

For harmonic excitation of the bimorph (i.e., $v(t)=V_0e^{j\omega t}$, where ω is the driving frequency and j is the unit imaginary number), the steady state response of Eq. (13) becomes

$$\eta_r(t) = \frac{-\chi_r V_0 e^{j\omega t}}{\omega_r{}^2 - \omega^2 + j2\zeta_r\omega_r\omega} \tag{16}$$

Physical steady state response of the beam is then obtained by substituting Eq. (16) into Eq. (7)

$$w(x,t) = \sum_{r=1}^{\infty}\frac{-\chi_r\phi_r(x)}{\omega_r{}^2 - \omega^2 + j2\zeta_r\omega_r\omega}V_0e^{j\omega t} \tag{17}$$

Hence, the steady state response of the beam at its free end is

$$w(L,t) = \sum_{r=1}^{\infty}\frac{-\chi_r\phi_r(L)}{\omega_r{}^2 - \omega^2 + j2\zeta_r\omega_r\omega}V_0e^{j\omega t} \tag{18}$$

3 Characterization of Unimorph Actuators

Twelve unimorphs are fabricated by bonding a MFC actuator to commercial sheet metal substrates with epoxy to validate the analytical model. Samples are bonded in vacuum bag to minimize the variation in the epoxy thickness and air gaps. Each sample employs a single M8507-P1 type MFC manufactured by Smart Material Inc., Germany, which use the d_{33} mode of piezoelectricity. Three different substrate materials with different thicknesses are studied. Total overhang length of the unimorphs are approximately 80 mm and the overhang length of the active area is set to be $L_{act}\cong 73$ mm during clamping. In order to accurately model the PZT fibers and the interdigitated electrodes, a sample of the (nonbonded) MFC 8507-P1 actuator is examined under a microscope (Fig. 2).

The measured values are cross-checked with the ones provided by the manufacturer, and the following values are used: thickness and width of each piezoceramic fiber are approximately 180 μm and 355 μm, respectively, and each epoxy layer between the fibers has a width of 51 μm. The total thickness of the active region of the MFC is $T_{MFC}=300$ μm, and therefore, each of the top and bottom Kapton layers in the active region is 60 μm thick. Since the total active width is approximately 7.3 mm, each sample has approximately 18 piezoceramic fibers, yielding a total piezoceramic width of $b_{pt}=6.4$ mm. The width of each electrode in the direction of the beam length is $u_e=97$ μm, and the spacing between the electrodes is $u_0=410$ μm. Therefore, the number of electrode pairs over the beam length is $N_e\cong 72$ (therefore, $\sim$144 electrode fingers), and the effective electrode spacing is about $\Delta_{el}=458.5$ μm. M8507-P1 uses Navy II piezoceramics, for which the effective value of the piezoelectric constant is approximately $e_{33}=19.1$ C/m^2.

Table 1 Thickness properties of each unimorph and its epoxy layer. MFC has a thickness of 0.30 mm.

Sample name	Substrate	Substrate thickness (mm)	Epoxy thickness (mm)
Br 1	Brass	0.0254	0.019
Br 2	Brass	0.0508	0.010
Br 3	Brass	0.0762	0.028
Br 4	Brass	0.1016	0.033
S 1	Steel	0.0254	0.008
S 2	Steel	0.0508	0.020
S 3	Steel	0.0762	0.018
S 4	Steel	0.1016	0.059
Al 2	Aluminum	0.0508	0.015
Al 3	Aluminum	0.0762	0.018
Al 4	Aluminum	0.1016	0.019
Al 5	Aluminum	0.1270	0.042

The substrate materials investigated are brass, stainless steel, and aluminum. The Young's moduli for these substrate materials are taken as 105 GPa, 200 GPa, and 70 GPa, respectively. The effective Young's modulus of the piezoceramic fibers is taken as 64 GPa. The epoxy type used for bonding the substrate and MFC layers is 3M DP460, and its shear strength is 4500 psi ($\sim$31 MPa). The substrate and average thicknesses of the epoxy layers between the substrate and the MFC layers are shown in Table 1. Note that the epoxy thickness has a variation of $\pm$0.02 mm. Epoxy thickness is an important source of uncertainty, and the values listed in the table are fine tuned by comparing the analytical first natural frequency (from Eq. (12)) and the experimental natural frequency when the system is close to short circuit conditions. This is not necessarily true because any amplifier that is used to actuate the MFC will have its own electrical dynamics. Such effects can be significant, but here, short circuit condition is assumed. The mass per length of the MFC and the epoxy layers is

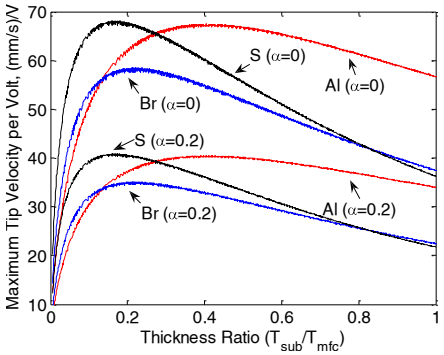

Fig. 3 Theoretical maximum tip-velocity response to harmonic excitation for a range of thickness ratios. Response corresponds to the first bending mode of a cantilever beam. T_{MFC} is 0.30 mm.

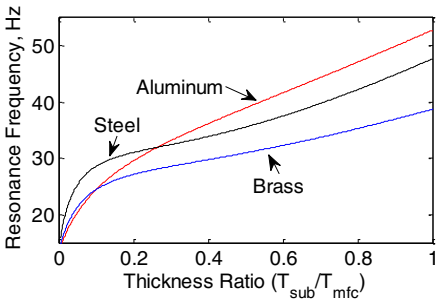

Fig. 4 Theoretical variation in the first bending mode frequency (in response to harmonic excitation) with substrate thickness and material

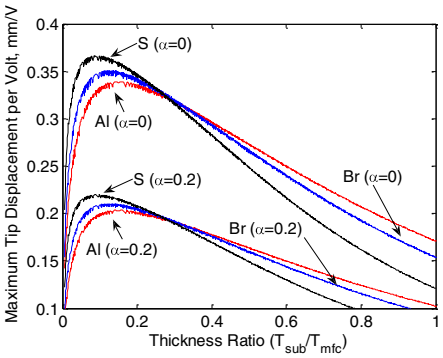

Fig. 5 Theoretical maximum tip displacement response to harmonic excitation for a range of thickness ratios. Response corresponds to the first bending mode of a cantilever beam. T_{MFC} is 0.30 mm.

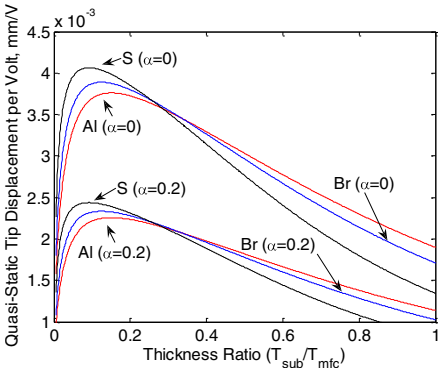

Fig. 6 Theoretical static tip displacement per volt for a range of thickness ratios. T_{MFC} is 0.30 mm.

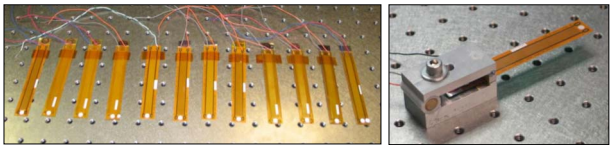

Fig. 7 Left: 12 unimorphs; right: one of the unimorphs clamped for testing

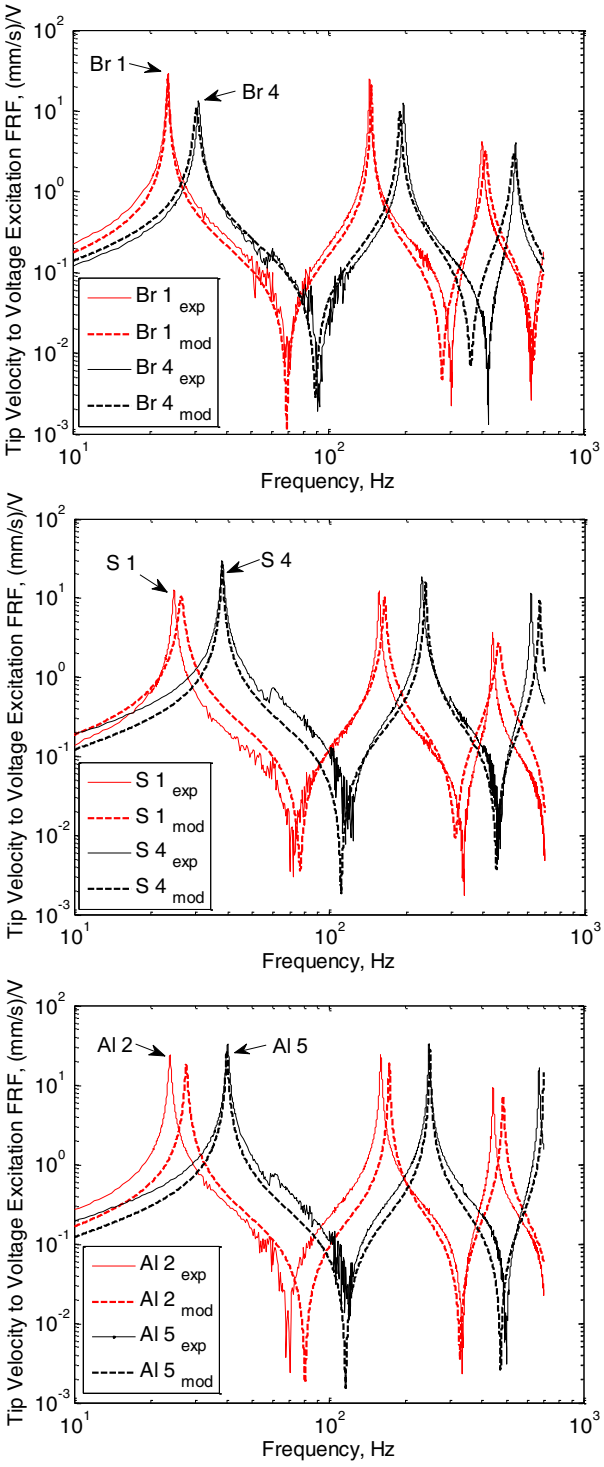

Fig. 8 Tip velocity to actuation FRF comparison of experiments to model for unimorphs

estimated experimentally as 0.0123 kg/m. The total mass per length of each sample is estimated by adding this value to the mass per length of each substrate. Here, the mass densities of the brass, steel, and aluminum substrates are taken as 9000 kg/m^3, 7800 kg/m^3, and 2700 kg/m^3, respectively.

A parametric study is conducted using the solution given in Eq. (18). MFC and epoxy properties are taken as previously reported, and a damping ratio of 0.005 is assumed for all modes. Solution is obtained for different Young's moduli and thickness ratios of the substrate with respect to the constant MFC thickness of 0.30 mm.

Table 2 Comparison of the experimental and predicted natural frequencies in Hz

	ω1_exp	ω1_mod	ω1%error	ω2_exp	ω2_mod	ω2%error	ω3_exp	ω3_mod	ω3%error
Al 2	23.8	27.6	16.0	160.0	172.9	8.1	441.9	484.0	9.5
Al 3	31.5	32.9	4.4	194.9	206.2	5.8	530.2	577.2	8.9
Al 4	34.3	34.2	−0.4	227.3	214.3	−5.7	612.8	600.1	−2.1
Al 5	40.1	39.8	−0.6	247.4	249.6	0.9	669.3	698.7	4.4
Br 1	23.7	23.6	−0.4	145.5	147.7	1.5	401.5	413.7	3.0
Br 2	25.5	25.4	−0.6	165.2	158.9	−3.8	454.4	445.0	−2.1
Br 3	29.1	28.9	−0.7	178.6	181.2	1.4	486.4	507.3	4.3
Br 4	31.1	30.6	−1.8	197.5	191.3	−3.1	543.2	535.8	−1.4
S 1	24.7	26.3	6.5	156.6	164.7	5.1	436.9	461.2	5.6
S 2	30.7	30.5	−0.5	192.2	191.1	−0.6	521.0	535.1	2.7
S 3	32.0	31.6	−1.3	200.6	197.7	−1.4	550.4	553.7	0.6
S 4	38.1	38.1	0.0	230.5	238.4	3.4	617.9	667.4	8.0

The effect of the empirical correction factor is also demonstrated. The tip-velocity-per-voltage (at the corresponding resonance frequency) is presented in Fig. 3.

It is important to note that the empirical correction factor (α) does not change the "optimum" thickness ratio, and that it is only an amplitudewise effect. The tip velocity shown is the maximum velocity achieved by the unimorph free end at its first resonance frequency. The effect of the empirical electric field correction factor (α) can also be seen. Note that the frequency of the maximum velocity (the first resonance frequency) changes from sample to sample because the moment of inertia and the mass per length are different between each sample. The variation in the first natural frequency is given in Fig. 4.

The tip-velocity data are integrated (assuming zero for the constant of integration) to get the maximum tip displacement, again at the corresponding resonance frequency. Figure 5 shows the displacements for the different materials and thickness ratios.

The effect of the material axial stiffness shows as a change in the maximum displacement (and the corresponding optimum thickness ratio). The steel substrate shows the highest displacement, however, at a thinner substrate when compared with aluminum substrate. Similar analysis is presented for static actuation (sufficiently below the first natural frequency), where the inertial effects simply vanish. The maximum tip displacement for static actuation of the unimorph actuators are presented in Fig. 6.

The results given in Fig. 6 for a unimorph actuator are modeled and experimentally verified in the literature [14]. As mentioned earlier, the value of α shifts the amplitude of displacement, but not the optimum thickness ratio. The model considers the linear, low-amplitude dynamic actuation, so the empirical α is not applicable for a static (and possibly geometrically nonlinear and hysteretic) high-voltage actuation.

The frequency response prediction of the model is compared with the experimental case for self-excited MFC unimorphs. Figure 7 presents the tested unimorph actuators and the clamp used for testing. A Polytec PDV-100 laser vibrometer is used to measure the tip velocity of the cantilevers, 79 mm from the clamped end. The actuators are excited with a 10 Vp-p pure sine tone generated by the data acquisition system. The excitation signal is buffered by a HP 3052 unity gain amplifier. A Siglab 20-42 data acquisition unit is used for the data processing.

Virtual sine sweep is used for frequency response function (FRF) measurements, where the excitation is a pure sine tone at constant frequency. The frequency is incremented only when transients are decayed from the previous frequency. Such method is utilized to avoid transients caused by more common (and faster) techniques, such as chirp excitation. The FRF is measured for tip-velocity-to-harmonic-voltage-excitation. Comparison of the model predictions and the experimental measurements are presented in Fig. 8. Note that only two thicknesses for each material are shown for plot clarity.

The FRFs presented shows the unimorphs with brass, steel, and aluminum substrates with two different thicknesses. The model predictions and the experimental results correlate very well. It must be noted that the bending stiffness used for the model is purely theoretical so there is a small mismatch between the experimental and the model prediction for the first natural frequency. One can "calibrate" the bending stiffness to match the prediction to the experimental values; however, such method is not utilized here. The prediction of the model for higher modes is simply a shift in the same direction relative to the shift observed in the first frequency. Considering the Euler–Bernoulli assumptions, this consistent shift is expected since it overpredicts the natural frequencies (due to effectively stiffer assumptions of the material behavior.) Table 2 shows a comparison of the first three natural frequency predictions to the experimental values for all 12 unimorphs.

The MFC actuated unimorph is a slender body; however, it includes nonlinearities due to the MFC's composite nature (including piezoceramic hysteresis.) The effect of hysteresis is frequency and amplitude dependent, and is not observed during the low-amplitude and high frequency experiments conducted in this paper. The nonuniform shear layer (at the epoxy interface) is also neglected here (due to low excitation voltages), which is another source of variance of the structure from the model assumptions. Considering that the predicted values are without any bending stiffness corrections, the model is capable of capturing the dynamics for a wide range of physical cases.

4 Conclusions and Future Work

This paper presented the modeling and experimental evaluation of MFC actuated unimorphs with brass, steel, and aluminum thicknesses with four different thicknesses. The linear electromechanical model successfully predicts the dynamic response for low actuation levels.

Embedded piezoceramics in structural and aerodynamic applications provide excellent shape manipulation. MFC actuators offer high flexibility and relatively large displacements for peak-to-peak actuation. Due to the nature of piezoceramics and important nonlinearity, material hysteresis arises for high-voltage actuation. Further experimental investigation needs to be conducted in order to determine the development of the hysteresis and to find the limits of the linear model proposed here.

Acknowledgment

This work was supported by the G. R. Goodson Professorship endowment. The authors would like to thank their colleagues at the Center for Intelligent Material Systems and Structures (CIMSS) for their support with the experiments and theoretical questions.

References

[1] Wilkie, W. K., Bryant, G. R., and High, J. W., 2000, "Low-Cost Piezocom-

posite Actuator for Structural Control Applications," Proceedings of the SPIE Seventh Annual International Symposium on Smart Structures and Materials, Newport Beach, CA.
[2] High, J. W. and Wilkie, W. K., "Method of Fabricating NASA-Standard Macro-Fiber Composite Piezoelectric Actuators," NASA Report Nos. TM-2003-212427 and ARL-TR-2833.
[3] Hagood, N. W., Kindel, R., Ghandi, K., and Gaudenzi, P., 1993, "Improving Transverse Actuation Using Interdigitated Surface Electrodes," Proceedings of the North American Conference on Smart Structures and Materials, Albuquerque, NM, SPIE Paper No. 1917-25, pp. 341–352.
[4] Williams, R. B., 2004, "Nonlinear Mechanical and Actuation Characterization of Piezoceramic Fiber Composites," Ph.D. thesis, Department of Mechanical Engineering, Virginia Tech, Blacksburg, VA.
[5] Glezer, A., Amitay, M., and Honohan, A., 2005, "Aspects of Low- and High-Frequency Actuation for Aerodynamic Flow Control," AIAA J., **43**(7), pp. 1501–1511.
[6] Pern, N. J., Jacob, J., and LeBeau, R., 2006, "Characterization of Zero Mass Flux Flow Control for Separation Control of an Adaptive Airfoil," Proceedings of the 36th Fluid Dynamics Conference, AIAA Paper No. 2006-3032.
[7] Ramakumar, K., and Jacob, J., 2005, "Flow Control and Lift Enhancement Using Plasma Actuators," Proceedings of the 35th Fluid Dynamics Conference, AIAA Paper No. 2005-4635.
[8] Kim, D. K., and Han, J. H., 2006, "Smart Flapping Wing Using Macro-Fiber Composite Actuators," Proc. SPIE, **6173**, pp. 1–9.
[9] Moses, R. W., Weisman, C. D., Bent, A. A., and Pizzochero, A. E., 2001, "Evaluation of New Actuators in a Buffet Loads Environment," Proceedings of the SPIE Eighth Annual International Symposium on Smart Structures and Materials, Newport Beach, CA.
[10] Bilgen, O., Kochersberger, K., Diggs, E. C., Kurdila, A. J., and Inman, D. J., 2007, "Morphing Wing Micro-Air-Vehicles via Macro-Fiber-Composite Actuators," Proceedings of the 48th AIAA/ASME/ASCE/AHS/ASC Structures, Structural Dynamics, and Materials Conference, Honolulu, HI, Apr. 23–26, Paper No. AIAA-2007-1785.
[11] Bilgen, O., Kochersberger, K., Diggs, E. C., Kurdila, A. J., and Inman, D. J., 2007, "Morphing Wing Aerodynamic Control via Macro-Fiber-Composite Actuators in an Unmanned Aircraft," Proceedings of the AIAA Infotech@Aerospace Conference, Rohnert Park, CA, May 7–10, Paper No. AIAA-2007-2741.
[12] Erturk, A., and Inman, D. J., 2008, "A Distributed Parameter Electromechanical Model for Cantilevered Piezoelectric Energy Harvesters," ASME J. Vibr. Acoust., **130**(4), p. 041002.
[13] Erturk, A., Bilgen, O., Fontenille, M., and Inman, D. J., 2008, "Piezoelectric Energy Harvesting From Macro-Fiber Composites With an Application to Morphing-Wing Aircrafts," Proceedings of the 19th International Conference on Adaptive Structures and Technologies, Ascona, Switzerland, Oct. 6–9.
[14] Inman, D. J., and Cudney, H. H., 1998, "Structural and Machine Design Using Piezoceramic Materials: A Guide for Structural Design Engineers," NASA Langley Final Report No. 20000044540.